Ultralow thermal conductivity in 1D and 2D imidazolium-based lead halide perovskites

Candida Pipitone, Stefano Boldrini, Alberto Ferrario, Gonzalo Garcìa-Espejo, Antonietta Guagliardi, Norberto Masciocchi, Antonino Martorana, Francesco Giannici, et al.

COLLECTIONS

Paper published as part of the special topic on New Solution-processed Perovskites and Perovskite-inspired Optoelectronic Materials and Devices

View Online   Export Citation   CrossMark

ARTICLES YOU MAY BE INTERESTED IN

Molecular passivation of MAPbI3 perovskite films follows the Langmuir adsorption rule
Applied Physics Letters **119**, 101101 (2021); https://doi.org/10.1063/5.0061818

Perspectives in flow-induced vibration energy harvesting
Applied Physics Letters **119**, 100502 (2021); https://doi.org/10.1063/5.0063488

Broadband low-frequency sound absorbing metastructures based on impedance matching coiled-up cavity
Applied Physics Letters **119**, 101901 (2021); https://doi.org/10.1063/5.0061012
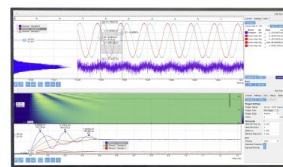
Applied Physics Letters

AIP Publishing

Ultralow thermal conductivity in 1D and 2D imidazolium-based lead halide perovskites

View Online   Export Citation   CrossMark

Candida Pipitone,[1] (iD) Stefano Boldrini,[2] (iD) Alberto Ferrario,[2] (iD) Gonzalo García-Espejo,[3] (iD) Antonietta Guagliardi,[4] (iD)
Norberto Masciocchi,[3] (iD) Antonino Martorana,[1] (iD) and Francesco Giannici[1,a)] (iD)

AFFILIATIONS

[1]Dipartimento di Fisica e Chimica "Emilio Segrè," Università di Palermo, viale delle Scienze, 90128 Palermo, Italy
[2]Institute of Condensed Matter Chemistry and Technologies for Energy (ICMATE), National Research Council (CNR), Corso Stati Uniti 4, 35127 Padova, Italy
[3]Dipartimento di Scienza e Alta Tecnologia & To.Sca.Lab., Università dell'Insubria, via Valleggio 11, 22100 Como, Italy
[4]Istituto di Cristallografia & To.Sca.Lab., Consiglio Nazionale delle Ricerche, via Valleggio 11, 22100 Como, Italy

Note: This paper is part of the APL Special Collection on New Solution-processed Perovskites and Perovskite-inspired Optoelectronic Materials and Devices.
a)Author to whom correspondence should be addressed: francesco.giannici@unipa.it

ABSTRACT

Low-dimensional hybrid organic–inorganic metal halide perovskites are rapidly emerging as a fascinating sub-class of the three-dimensional parent structures, thanks to their appealing charge and thermal transport properties, paired to better chemical and thermal stabilities. Extensive investigations of the thermal behavior in these systems are of paramount relevance to understand their optoelectronic and thermo-electric applications. Herein, we present a complete thermophysical characterization of imidazolium lead iodide, $(IMI)PbI_3$, a 1D pseudo-perovskite with chains of face-sharing octahedra, and histammonium lead iodide, $(HIST)PbI_4$, a 2D layered perovskite with corner-sharing octahedra. Upon heating, the two compounds show highly anisotropic thermal expansion effects and high thermal stability until 250–300 °C. The thermal diffusivity of pelletized powders was measured with the laser flash technique from room temperature up to 225 °C. To account for the reduced density of the pelletized powders with respect to the bulk, the diffusivity data in different atmospheres were modeled as a function of the volume fraction and dimensionality of the pores, allowing to extrapolate the thermal conductivity of the bulk materials. The two compounds exhibit an ultralow thermal conductivity of 0.15 W/m K, two to three times lower than that reported on 3D $MAPbI_3$ using the same technique. This finding suggests the primary role of the organic molecules within the hybrid systems, regardless of the octahedra connectivity and dimensionality.

The thermal and electrical transport properties of hybrid lead halide perovskites with low dimensionality were not reported until very recently.[1–5] The interest for these compounds is rapidly blooming since they often display very favorable chemical stability to air and moisture, if compared to the prototypical $(MA)PbI_3$ or $(FA)PbI_3$ species, thus representing a promising route to achieve air-stable electrical conductors with low thermal conductivity. In this context, the use of the "perovskite" term for "low-dimensional" materials not showing the extended 3D network of corner-sharing octahedra—and often displaying a different kind of connectivity of the inorganic scaffold—is currently under debate.[6] For the sake of clarity, herein, we apply the term *perovskite* to indicate halometalates, where a sub-network of *corner*-sharing octahedra (2D layers or 1D chains) is present, whereas

the term *pseudo-perovskite* is used for those compounds based on edge- or face-sharing octahedra (2D, 1D) sub-networks or even for 0D moieties.

Recently, lower-dimensional (pseudo-)perovskites have been inserted in 2D/3D and 1D/3D heterostructures for photovoltaic devices, showing improved performances.[7–9] Ultralow thermal conductivities of 2D metal halide perovskites with various ammonium-based organic cations were measured (by time domain thermoreflectance) in the 0.10–0.19 W/m K range and mainly attributed to the relative orientation of the organic chains between the inorganic layers without any influence of their thicknesses. These values are up to five times lower than in the 3D $(MA)PbI_3$ counterpart. In this regard, a more comprehensive evaluation of the thermal properties, which include conductivity, phase

stability, and thermal strain, would greatly foster advances in the field of low-dimensional perovskites and pseudo-perovskites, since they are critical in assembling well-designed devices with a long lifespan.[10] Moreover, the low-dimensionality criterion can lead to the design of new thermoelectric materials.[11]

Aromatic heterocycles like simple or substituted imidazoles readily form hybrid halide perovskites through precipitation from hot acidic aqueous solutions containing the PbX_2 precursor (X = I, Br). The presence of substituents on the imidazole ring and the charge of the resulting cation eventually determine the dimensionality of the perovskite: $(IMI)PbI_3$, based on the monovalent imidazolium cation, has a 1D structure with chains of face-sharing PbI_6 octahedra (Fig. 1) with heterocyclic ring axis perpendicular to the haloplumbate chains. Due to the presence of an additional basic side chain on the imidazole ring, a divalent cation is formed by complete protonation of histamine. In $(HIST)PbI_4$, histammonium lies flat between perovskite monolayers of corner-sharing PbI_6 octahedra (Fig. 1), leading to a 2D structure. The two systems under study differ mainly on the dimensionality and connectivity of the haloplumbate sub-networks, and also in the size and shape of the organic cations, both based on five-membered heterocyclic rings. Thus, they are chemically, but not structurally, related.

Both these materials have recently shown interesting functional properties. $(IMI)PbI_3$ incorporation in $(CH_3NH_3)PbI_3$ thin films improved the morphology, stability, and performance of the 1D/3D heterostructure.[12] $(HIST)PbI_4$ thin films displayed a perpendicular, rather than parallel, layer orientation with respect to the substrate, a geometrical arrangement, which is more favorable for improving the performances of solar cells.[13] An appraisal of the thermal properties of the two compounds is of great relevance for applications in photovoltaics (here, phase/thermal stability and thermal stress under illumination are highly critical issues), or in the thermoelectric field, where a very low thermal conductivity is a must.
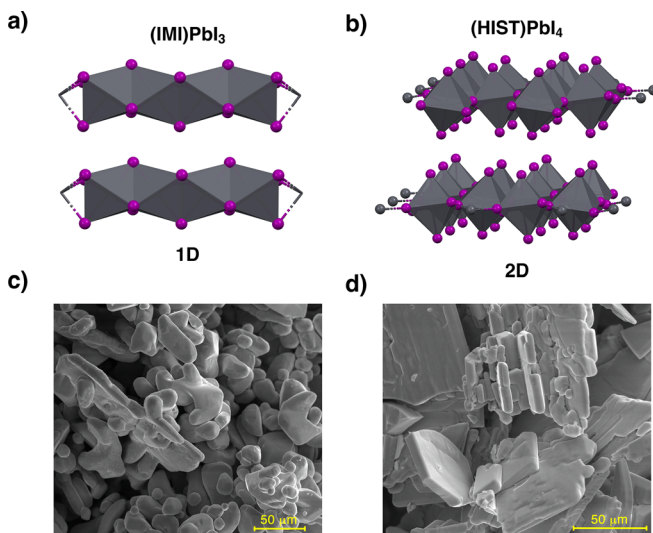
The thermal diffusivity of hybrid perovskite materials is usually measured using time-domain thermoreflectance at room temperature on single crystal specimens. Even if this technique recently evolved to permit in-plane thermal diffusivity measurements, it is generally used for through-plane analysis.[1,4] Together with the intrinsic anisotropy of low-dimensional structures, this provides only a limited insight on thermal conductivity, especially for applications that require higher temperatures. Recently, laser flash analysis (LFA) was also employed to characterize the thermal diffusivity of polycrystalline samples of $(CH_3NH_3)PbI_3$.[5]

In this Letter, we present an extensive study of the thermal properties (conductivity, phase stability, and thermal-induced strain) of $(IMI)PbI_3$ and $(HIST)PbI_4$ powders, both species displaying extremely low thermal conductivity values. In order to prevent possible degradation or polymorphic phase changes induced by heating above 250 °C, samples were pelletized at room temperature. The subsequent application of LFA, a consolidated and versatile technique, is the first example on samples compacted at room temperature. Through the LFA measurements in different atmospheres, we discuss the application of two microstructural models accounting for the residual, and unavoidable, contribution of pores still present in the compacted pellets to the thermal conductivity.

The phase stability (up to 300 °C) and thermal-induced lattice strains are investigated by thermogravimetric and thermodiffractometric measurements, complementing the thermal diffusivity data.
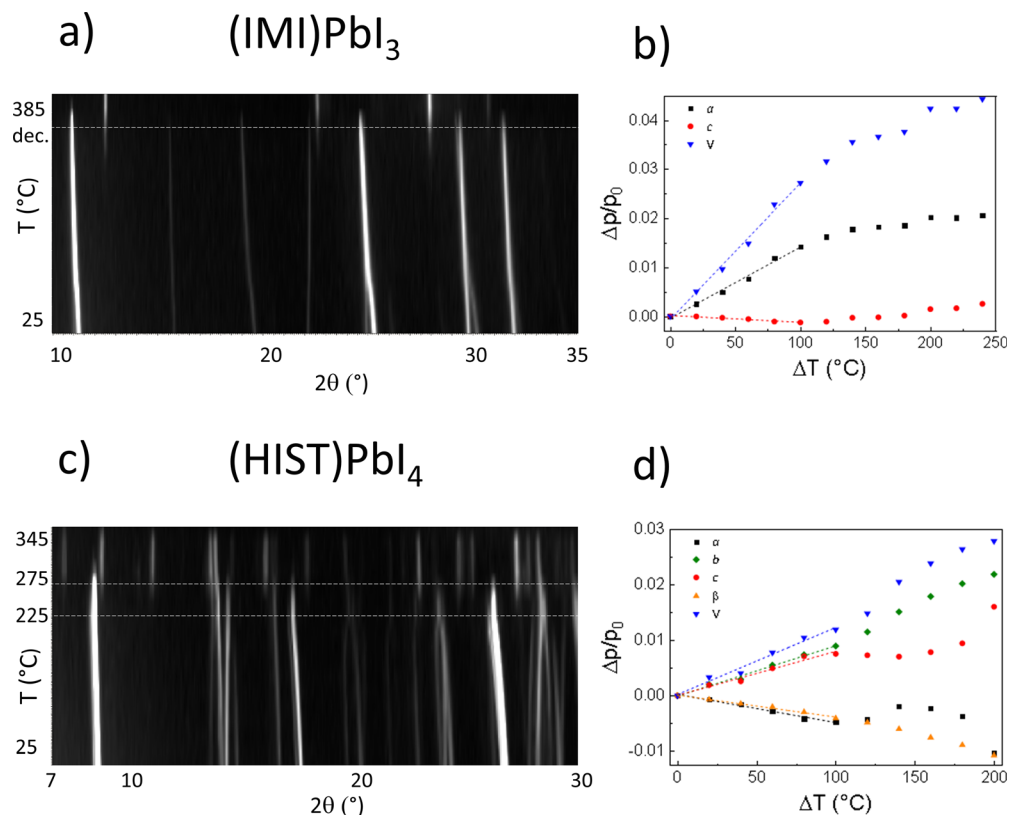
$(IMI)PbI_3$ and $(HIST)PbI_4$ powders were synthesized from a hot aqueous HI solution containing lead oxide and imidazole or histamine, leading to the immediate precipitation of fine yellow and orange powders for $(IMI)PbI_3$ and $(HIST)PbI_4$, respectively. XRD confirmed the phase purity according to the published structures[13,14] (Fig. S1).

The decomposition temperature, estimated by thermogravimetry (Fig. S2), was taken as a reference for further measurements: samples show substantial phase stability up to 250 °C (for $(IMI)PbI_3$) or 300 °C (for $(HIST)PbI_4$). This stability is comparable to 3D perovskites, as $(MA)PbI_3$ measured in similar conditions decomposes around 250 °C (Fig. S2c).

Variable-temperature x-ray diffraction (VT-XRD) provides a clear picture of the crystal phases [Figs. 2(a), 2(c), and S3] and lattice parameters' [Figs. 2(b) and 2(d)] evolution upon raising the temperature, well before thermal decomposition. For $(IMI)PbI_3$, the hexagonal crystal structure remains stable up to decomposition [Fig. 2(a), dashed horizontal line]; for $(HIST)PbI_4$, a progressive change associated with thermal expansion is visible in Fig. 2(c), followed by the merging of several couples of peaks, in line with a second-order phase transition (where a new state of *increased symmetry* develops continuously from the ordered low temperature phase), leading to an orthorhombic polymorph of *Cmcm* symmetry. Finally, a high-temperature (still unidentified) crystal phase suddenly appears above 275 °C.

For both materials under study, refinement of cell parameters at different temperatures allowed the anisotropic thermal expansion coefficients to be derived (Table I), using their relative variations, $\Delta p/p_0$, with p = *a, b, c*, and β, and p_0 being the reference value at room temperature. The $\Delta p/p_0$ values are reported in Figs. 2(b) and 2(c) as a function of the temperature, and the visualization of the thermal strain tensors is shown in Fig. S4.

In $(IMI)PbI_3$ (hexagonal symmetry), the *c* axis remains almost constant. As expected from its 1D structural motif, the haloplumbate

FIG. 1. $(IMI)PbI_3$ (left) and $(HIST)PbI_4$ (right): sketch of the connectivity of the PbI_6 octahedra (top) and representative particle shapes from SEM imaging (bottom). Scale bar = 50 μm. For the sake of clarity, organic cations are omitted from the sketches.

FIG. 2. VT-XRD plots for (IMI)PbI$_3$ (a) and (HIST)PbI$_4$ (c), highlighting the relative changes of the peak positions, their merging, and the formation of PbI$_2$ (a) or of a still unknown crystal phase (c) at high temperatures; in (b) and (d): relative variations of the cell parameters of (IMI)PbI$_3$ (b) and (HIST)PbI$_4$ (d) as a function of temperature increase with respect to room temperature. Linear regimes up to 125 °C are shown, the slope of which corresponds to the linear (or volumetric) thermal expansion coefficients. The countercorrelated a and c variations in the high-temperature regime [panel (d)] are likely attributed to numerical instability of the refinement, as the primitive monoclinic metrics approach the C-centered orthorhombic one (see the supplementary material).

chains within (IMI)PbI$_3$, stretching out in the c direction, are only marginally changed (and actually shrink) upon mild heating, in line with what already found in other 1D perovskites.[15] Two different thermal expansion coefficient regimes, within the same crystal phase and with markedly different slopes, are then identified in (IMI)PbI$_3$, below and above 120 °C. These are attributed to the progressive increase in the vibrational freedom (including ring libration), until additional high-energy modes (likely, wheel-like rotations of the imidazolium cation) are

TABLE I. Linear and volumetric thermal expansion coefficients derived from VT-XRD data collected in the 25–125 °C range. Here, α_p is derived from the linear regression of $\Delta p/p_0$ vs ΔT, as in $\Delta p/p_0 = \alpha_p \Delta T$.

Parameter	(IMI)PbI$_3$ α (10^{-6} K^{-1})	(HIST)PbI$_4$ α (10^{-6} K^{-1})
a	145	50
b	145	90
c	−14	79
β	0	−39
V	277	121

activated. This interpretation is in line with the observed behavior of bis-carboxylate imidazolium salts, where progressively increasing libration amplitudes (near the kHz regime), up to heavy orientational disordering above 100 °C, were detected by several complementary experimental techniques (e.g., NMR, impedance spectroscopy, and variable-temperature single-crystal x-ray crystallography).[16] In (IMI)PbI$_3$, where no strong directional H-bonds between the imidazolium ring and the iodine atoms of the 1D framework are at work [the shortest NH···I contact being 3.95(6) Å at 150 K (Ref. 14)], the onset of these motions within the solid is expected to be further favored.

For (HIST)PbI$_4$, below 225 °C, two thermal expansion coefficient ranges are identified [see Fig. 2(d)]: a linear regime is evidenced only below 100 °C with more complex and correlated changes of the cell axes being observed above this temperature up to the clear transition providing a markedly distinct (still uninterpreted) XRD pattern.

For both samples, the thermal expansion coefficients determined from the low temperature regimes (from 25 to 125 °C) are summarized in Table I. Since the porosity of our materials, as discussed below, refers uniquely to the presence of voids between amassed crystallites (as per the SEM images of Fig. 1), and not to intrinsic crystal structure porosity (as in the case of zeolites, MOFs and COFs), the occasional presence of molecular absorbates contaminating the samples cannot

have a direct structural effect. Therefore, the observed cell parameter changes are the clear manifestation of the stiffness/compliance of the interatomic contacts within (tiny) dense crystalline monoliths.

From the cell volume variations between 25 and 225 °C, the relative changes in density are −0.043 for (IMI)PbI$_3$ and −0.027 for (HIST)PbI$_4$, respectively. On the other hand, neglecting the thermal expansion results in an underestimation at higher temperatures of the measured thermal diffusivity (by laser flash analysis) that is proportional to the square of the linear expansion. For the reasons above, thermal expansion was neglected in the following.

Thermal diffusivity measurements, when carried out in vacuum or in He and Ar atmospheres (Fig. 3), resulted in extremely low values, down to 0.04 and 0.07 W/m K, which are a tell-tale sign of a systematic underestimation. Such an effect can be ascribed to porosity, as the thermal conductivity of the gas employed during measurements can, indeed, affect the correct estimate of thermal diffusivity. The underestimation is particularly significant when the solid material and the pores possess "comparable" thermal conductivity values, as in the present case: indeed, the extremely low thermal conductivity shown by hybrid perovskites [17] does not usually differ by more than one order of magnitude from that of air.

Measurements were then carried out in He and Ar atmosphere to assess the role of the porosity. The significant difference in thermal conductivity acquired in different atmospheres indicates that a substantial fraction of the porosity is effective (or open) porosity. The variation of the measured thermal diffusivity as a function of the atmosphere also allows us to validate different geometrical models of porosity, leading to a self-consistent microstructural model that fits all the various diffusivity values in different environments. Thermal conductivity data of (IMI)PbI$_3$ and (HIST)PbI$_4$ samples measured in vacuum, He, and Ar atmosphere at room temperature are reported in Fig. 3. Measurements in Ar were also carried out as a function of
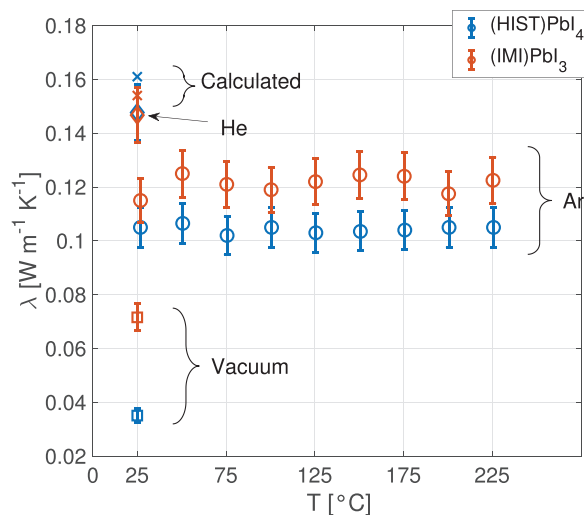
FIG. 3. Thermal conductivity of (IMI)PbI$_3$ and (HIST)PbI$_4$ measured in the 25–225 °C temperature range under Ar (○), and at 25° C under He (◇), or in vacuum (□). The calculated room-temperature conductivity values for the bulk materials (×) are also reported. RT values with different atmospheres are reported in the supplementary material. Error bars represent 7% measurement error.

temperature up to 225 °C, resulting in a nearly constant value of 0.12 W/m K for (IMI)PbI$_3$ and 0.11 W/m K for (HIST)PbI$_4$.

The microscopy images of the pressed samples (Figs. S5 and S6) revealed dispersed pores in an apparently continuous material matrix. This microstructure is usually referred to as *asymmetric configuration*.[18]

Considering the porosity as a second phase, the thermal conductivity λ_c of the composite is expressed by the matrix (λ_M) and pores (λ_g) thermal conductivities by the Maxwell–Garnet model,[19] which considers randomly oriented dispersed ellipsoid pores

$$\lambda_c = \lambda_M \frac{L\lambda_g + (1-L)\lambda_M + f(1-L)(\lambda_g - \lambda_M)}{L\lambda_g + (1-L)\lambda_M - fL(\lambda_g - \lambda_M)}, \quad (1)$$

where f is the volumetric fraction of pores and L is the depolarization factor of the ellipsoids in the direction of heat flow[20] with values between 0 and 1 depending on the ellipsoid shape.

Under the hypothesis that most of the porosity is open, Eq. (1) holds for all atmospheres with the same value for L (which only depends on the geometry) and λ_M of the material. From the relative density of samples, the volumetric fraction of pores, f, is 0.146 for (HIST)PbI$_4$ and 0.107 for (IMI)PbI$_3$. Solving Eq. (1) for λ_M for the two atmospheres and imposing the identity of the two expressions for λ_M lead to $\lambda_M^{(HIST)PbI4} = 0.16 \pm 0.01$ W/mK and $\lambda_M^{(IMI)PbI3} = 0.16 \pm 0.01$ W/mK. Also, the calculated conductivity values for the dense materials are, thus, equivalent. Self-consistent solutions for Eq. (1) lead to values of L that are compatible with oblate spheroids for (HIST)PbI$_4$ and (IMI)PbI$_3$: $L = 0.80$ and $L = 0.78$, respectively. This finding agrees with the morphology of the starting powders, mainly composed of lamellar-shaped grains, more pronounced in the case of (HIST)PbI$_4$ (see Fig. 1), and the uniaxial pressing used to produce the measured pellets. The above model can be further refined to take into account the possible preferential orientation of these oblate spheroids[21]

$$1 - f = \left(\frac{\lambda_M}{\lambda_c}\right)^\varsigma \frac{\lambda_g - \lambda_c}{\lambda_g - \lambda_M} \left(\frac{\lambda_c + \gamma\lambda_g}{\lambda_M + \gamma\lambda_g}\right)^\eta, \quad (2)$$

where the parameters ς, γ, and η depend on the shape factor of the spheroids, F, and their symmetry, α. (Their complete explanation is provided in the supplementary material.) The image analysis of the pores shape and orientation (not reported) results in a large distribution of α around about 0°, at least for the (HIST)PbI$_4$ sample. While Eq. (2) cannot be solved directly, a numerical method was used to obtain λ_M as a function of F with the assumption that $\alpha = 0°$. The curves of numerical solutions for Ar and He are reported in Fig. S7 for both (IMI)PbI$_3$ and (HIST)PbI$_4$.

Eventually, from this model, it is possible to extrapolate the thermal conductivity value for the fully dense bulk sample: the λ_M and F values that verify Eq. (2) at the same time for the He and Ar measurements correspond to the thermal conductivity of the sample in the full-dense limit. Thermal conductivity of the composite as a function of the porosity fraction as obtained from Eqs. (1) and (2) (a numerical solution) is reported in Fig. 4. Markers indicate experimental values of porous materials, whereas the y-intercepts represent the thermal conductivity of the matrix, λ_M, i.e., without the porosity effect.

The values estimated for λ_M are remarkably the same (within errors) as what obtained with the previous model [Eq. (1)], and the
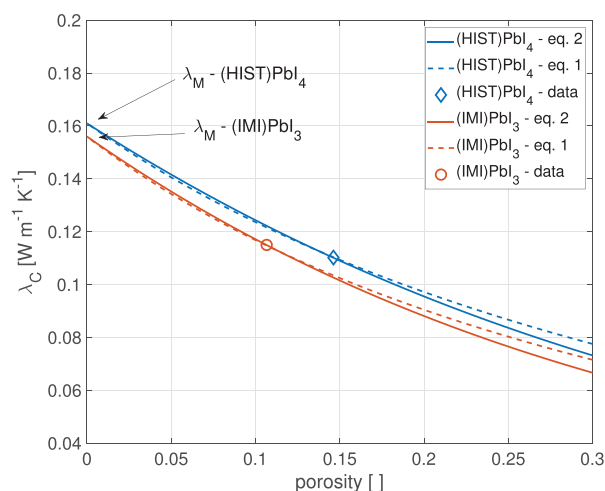
FIG. 4. Calculated dependence on the porosity fraction of the room-temperature thermal conductivity obtained from Eqs. (1) and (2) for $(HIST)PbI_4$ and $(IMI)PbI_3$. Measured values under Ar atmosphere are also reported.

shape factor F is around 0.12 for both materials, confirming the shape of the pores obtained previously.[21]

The extrapolated bulk limit values for the thermal conductivity obtained with the procedure outlined above are 0.16 ± 0.01 W/m K for both samples, therefore, comparable to those reported very recently for two-dimensional lead iodide hybrid perovskite thin films[22] and single crystals.[1] Indeed, while bulk 3D lead halide perovskites possess thermal conductivities as low as 0.35 W/m K (with larger values measured for the Cs^+-containing species than for methylammonium), the presence of iodides and the low dimensionality of pseudo-perovskites foster an additional lowering, down to the 0.10 W/m K regime.[23] It should be noted, however, that, in the case of linear alkylammonium chains separating the lead iodide layers, the chain length has a very marginal impact on thermal conductivity, while the relative orientation of the crystal domain (and then of the chains themselves) was found to be very important for reducing the thermal transport.

Significant differences were reported out of macroscopic investigations for the heat transfer obtained between powder and bulk (i.e., full density) samples, generically attributed to the presence of defects in the powder particles. In this work, we determined bulk values by extrapolating the heat transfer properties at different porosity values, which should make them comparable to the ultralow thermal conductivity of single-crystal specimens. The peculiar thermal properties of these materials, that is, their notoriously low thermal conductivities and high thermal expansion coefficients, suggest that proper thermal management in devices will be important to overcoming some current limitations.

In the present case, the thermal transport properties are essentially determined by the nature of the heterocycle cations between chains, regardless of the perovskite framework connectivity and dimensionality and can eventually be traced back to the dynamic disordering effects of the cations, increasing (at least locally) the "average" point group symmetry. Indeed, experimental[11,24] and theoretical[25] reports on $(MA)PbI_3$ have already focused on the orientational

disorder of the cations, to which the ultralow thermal conductivity is attributed. While a more detailed comparative analysis of this rapidly growing field has been reviewed very recently,[17] suffice here to say, that similar interpretations (based on the cation dynamics) have been reported for 2D[22] systems, suggesting the active nature of rattling moieties hosted in the inter-haloplumbate voids. In this respect, the evaluation of thermal conductivity mechanisms from first principles (*ab initio* or with empirical molecular dynamics), or through ancillary experimental evidence (e.g., variable temperature NMR or neutron scattering studies) may further help in rationalizing the relations between the structure and properties in such diverse compounds.[26,27]

The ultralow thermal conductivity of these compounds is attributed to efficient phonon scattering by the highly mobile organic cations, the structure, and dynamics of which confirm earlier studies on disordered materials to be possibly used in the thermoelectric field.[17,28,29] However, these phonon scatterers adversely reduce electrical conductivity as well. Therefore, the work can be anticipated in the direction of preparing composites of crystalline organic semiconductors, in which $(IMI)PbI_3$ and $(HIST)PbI_4$ particles are dispersed and act as phonon scatterers, while maintaining the high electronic conductivity of the host matrix. Indeed, such a strategy has been already proposed with a number of fully organic or inorganic fillers (carbon nanotubes, nanosized metal tellurides),[30,31] but not yet with low-dimensional hybrid pseudo-perovskite halometalates.

See the supplementary material for the detailed description of syntheses and characterization methods, thermogravimetric and VT-XRD data, thermal expansion tensors, and numerical solutions of Eq. (2).

DATA AVAILABILITY

The data that support the findings of this study are available from the corresponding author upon reasonable request.

REFERENCES

[1]M. A. J. Rasel, A. Giri, D. H. Olson, C. Ni, P. E. Hopkins, and J. P. Feser, "Chain-length dependence of thermal conductivity in 2D alkylammonium lead iodide single crystals," ACS Appl. Mater. Interfaces **12**, 53705–53711 (2020).

[2]N. Hoshino, S. Tamura, and T. Akutagawa, "Negative-to-positive thermal conductivity temperature coefficient transition induced by dynamic fluctuations of the alkyl chains in the layered complex $(C_4H_9NH_3)_2CuCl_4$," Chem. Eur. J. **26**, 2610–2618 (2020).

[3]C. Li, H. Ma, T. Li, J. Dai, M. A. J. Rasel, A. Mattoni, A. Alatas, M. G. Thomas, Z. W. Rouse, A. Shragai, S. P. Baker, B. J. Ramshaw, J. P. Feser, D. B. Mitzi, and Z. Tian, "Remarkably weak anisotropy in thermal conductivity of two-dimensional hybrid perovskite butylammonium lead iodide crystals," Nano Lett. **21**, 3708–3714 (2021).

[4]A. D. Christodoulides, P. Guo, L. Dai, J. M. Hoffman, X. Li, X. Zuo, D. Rosenmann, A. Brumberg, M. G. Kanatzidis, R. D. Schaller, and J. A. Malen, "Signatures of coherent phonon transport in ultralow thermal conductivity two-dimensional Ruddlesden–Popper phase perovskites," ACS Nano **15**, 4165–4172 (2021).

[5]X. Long, Z. Pan, Z. Zhang, J. J. Urban, and H. Wang, "Solvent-free synthesis of organometallic halides $CH_3NH_3PbI_3$ and $(CH_3NH_3)_3Bi_2I_9$ and their thermo-electric transport properties," Appl. Phys. Lett. **115**, 072104 (2019).

[6]N. Mercier, "Hybrid halide perovskites: Discussions on terminology and materials," Angew. Chem. Int. Ed. **58**, 17912–17917 (2019).

[7]M. Parashar, R. Singh, K. Yoo, and J.-J. Lee, "Formation of 1-D/3-D fused perovskite for efficient and moisture stable solar cells," ACS Appl. Energy Mater. **4**, 2751–2760 (2021).

[8]M. M. Elsenety, M. Antoniadou, N. Balis, A. Kaltzoglou, L. Sygellou, A. Stergiou, N. Tagmatarchis, and P. Falaras, "Stability Improvement and performance reproducibility enhancement of perovskite solar cells following $(FA/MA/Cs)PbI_{3-x}Br_x/(CH_3)_3SPbI_3$ dimensionality engineering," ACS Appl. Energy Mater. **3**, 2465–2477 (2020).

[9]E.-B. Kim, M. S. Akhtar, H.-S. Shin, S. Ameen, and M. K. Nazeeruddin, "A review on two-dimensional (2D) and 2D-3D multidimensional perovskite solar cells: Perovskites structures, stability, and photovoltaic performances," J. Photochem. Photobiol. C **48**, 100405 (2021).

[10]G. Divitini, S. Cacovich, F. Matteocci, L. Cinà, A. Di Carlo, and C. Ducati, "In situ observation of heat-induced degradation of perovskite solar cells," Nat. Energy **1**, 15012 (2016).

[11]A. Pisoni, J. Jaćimović, O. S. Barišić, M. Spina, R. Gaál, L. Forró, and E. Horváth, "Ultra-low thermal conductivity in organic–inorganic hybrid perovskite $CH_3NH_3PbI_3$," J. Phys. Chem. Lett. **5**, 2488–2492 (2014).

[12]Y. Zhang, G. Grancini, Z. Fei, E. Shirzadi, X. Liu, E. Oveisi, F. F. Tirani, R. Scopelliti, Y. Feng, M. K. Nazeeruddin, and P. J. Dyson, "Auto-passivation of crystal defects in hybrid imidazolium/methylammonium lead iodide films by fumigation with methylamine affords high efficiency perovskite solar cells," Nano Energy **58**, 105–111 (2019).

[13]L. Mao, H. Tsai, W. Nie, L. Ma, J. Im, C. C. Stoumpos, C. D. Malliakas, F. Hao, M. R. Wasielewski, A. D. Mohite, and M. G. Kanatzidis, "Role of organic counterion in lead- and tin-based two-dimensional semiconducting iodide perovskites and application in planar solar cells," Chem. Mater. **28**, 7781–7792 (2016).

[14]O. J. Weber, K. L. Marshall, L. M. Dyson, and M. T. Weller, "Structural diversity in hybrid organic–inorganic lead iodide materials," Acta Cryst. B **71**, 668–678 (2015).

[15]C. Pipitone, F. Giannici, A. Martorana, F. Bertolotti, G. Calabrese, S. Milita, A. Guagliardi, and N. Masciocchi, "Proton sponge lead halides containing 1D polyoctahedral chains," CrystEngComm **23**, 1126–1139 (2021).

[16]Y. Sunairi, S. Dekura, A. Ueda, T. Ida, M. Mizuno, and H. Mori, "Anhydrous purely organic solid-state proton conductors: Effects of molecular dynamics on the proton conductivity of imidazolium hydrogen dicarboxylates," J. Phys. Soc. Jpn. **89**, 051008 (2020).

[17]M. A. Haque, S. Kee, D. R. Villalva, W. Ong, and D. Baran, "Halide perovskites: Thermal transport and prospects for thermoelectricity," Adv. Sci. **7**, 1903389 (2020).

[18]F. Cernuschi, S. Ahmaniemi, P. Vuoristo, and T. Mäntylä, "Modelling of thermal conductivity of porous materials: Application to thick thermal barrier coatings," J. Eur. Ceram. Soc. **24**, 2657–2667 (2004).

[19]A. Bjorneklett, L. Haukeland, J. Wigren, and H. Kristiansen, "Effective medium theory and the thermal conductivity of plasma-sprayed ceramic coatings," J. Mater. Sci. **29**, 4043–4050 (1994).

[20]P. N. Sen, C. Scala, and M. H. Cohen, "A self-similar model for sedimentary rocks with application to the dielectric constant of fused glass beads," Geophysics **46**, 781–795 (1981).

[21]F. Cernuschi, P. Bison, and A. Moscatelli, "Microstructural characterization of porous thermal barrier coatings by laser flash technique," Acta Mater. **57**, 3460–3471 (2009).

[22]A. Giri, A. Z. Chen, A. Mattoni, K. Aryana, D. Zhang, X. Hu, S.-H. Lee, J. J. Choi, and P. E. Hopkins, "Ultralow thermal conductivity of two-dimensional metal halide perovskites," Nano Lett. **20**, 3331–3337 (2020).

[23]T. Haeger, R. Heiderhoff, and T. Riedl, "Thermal properties of metal-halide perovskites," J. Mater. Chem. C **8**, 14289–14311 (2020).

[24]A. C. Ferreira, A. Létoublon, S. Paofai, S. Raymond, C. Ecolivet, B. Rufflé, S. Cordier, C. Katan, M. I. Saidaminov, A. A. Zhumekenov, O. M. Bakr, J. Even, and P. Bourges, "Elastic softness of hybrid lead halide perovskites," Phys. Rev. Lett. **121**, 085502 (2018).

[25]A. Mattoni, A. Filippetti, M. I. Saba, and P. Delugas, "Methylammonium rotational dynamics in lead halide perovskite by classical molecular dynamics: The role of temperature," J. Phys. Chem. C **119**, 17421–17428 (2015).

[26]L. Lindsay, C. Hua, X. L. Ruan, and S. Lee, "Survey of ab initio phonon thermal transport," Mater. Today Phys. **7**, 106–120 (2018).

[27]X. Qian, X. Gu, and R. Yang, "Thermal conductivity modeling of hybrid organic-inorganic crystals and superlattices," Nano Energy **41**, 394–407 (2017).

[28]Y. Wang, R. Lin, P. Zhu, Q. Zheng, Q. Wang, D. Li, and J. Zhu, "Cation dynamics governed thermal properties of lead halide perovskite nanowires," Nano Lett. **18**, 2772–2779 (2018).

[29]N. P. Gallop, O. Selig, G. Giubertoni, H. J. Bakker, Y. L. A. Rezus, J. M. Frost, T. L. C. Janesn, R. Lovrincic, and A. A. Bakulin, "Rotational cation dynamics in metal halide perovskites: Effect on phonons and material properties," J. Phys. Chem. Lett. **9**, 5987–5997 (2018).

[30]G. P. Moriarty, K. Briggs, B. Stevens, C. Yu, and J. C. Grunlan, "Fully organic nanocomposites with high thermoelectric power factors by using a dual-stabilizer preparation," Energy Technol. **1**, 265–272 (2013).

[31]G. Prunet, F. Pawula, G. Fleury, E. Cloutet, A. J. Robinson, G. Hadziioannou, and A. Pakdel, "A review on conductive polymers and their hybrids for flexible and wearable thermoelectric applications," Mater. Today Phys. **18**, 100402 (2021).